

References and Notes

1. *U.S. Geol. Surv. Prof. Pap.* 1250 (1981).
2. C. S. Weaver and S. D. Malone, personal communication.
3. According to U. S. Weather Service radar at Portland, the eruption column reached its maximum height, 11.5 km above the vent, at 1930 P.S.T. Maximum radar reflection lasted only 5 minutes; the plume then gradually descended and drifted south-southeast. Pumice in flow deposits in and north of the crater appears identical to that which fell from the plume onto the south flank of the volcano.
4. D. A. Swanson, personal communication. A small part of the dome low on the south sector disappeared during the eruption as a result of explosion or collapse; this location may mark the approximate position of the principal vent.
5. Velocity is calculated from superelevation flood surfaces at channel bends by the formula $v^2 = rg \tan \theta$, where v is the velocity of ideal fluid, r is the radius of curvature at the bend, g is the acceleration due to gravity, and θ is the angle between the superelevated flow surface and the horizontal, measured normal to the flow direction.
6. *Fahrböschung* is given by $\arctan(H/L)$, where H is the maximum vertical fall and L is the maximum horizontal runout [A. Heim, *Bergsturz und Menschenleben*, Fretz und Wasmuth, Zurich, 1932]. The parameter has been used by Heim and by others as an index of the average apparent coefficient of friction: $f = H/L$ [W. G. Parisseau and B. Voight, in *Rockslide and Avalanches*, B. Voight, Ed. (Elsevier, Amsterdam, 1979), vol. 2, pp. 6-8]. By comparison, debris avalanches at Sherman Glacier, Gros Ventre, and Mount St. Helens (18 May 1980) have *fahrböschung*-derived coefficients of friction of 0.22, 0.17, and 0.09 to 0.15, respectively.
7. K. J. Hsü, *Geol. Soc. Am. Bull.* 86, 129 (1975).
8. Hydraulic ponding occurs in an unblocked open channel if water is supplied more rapidly than it can be discharged; water level therefore rises until outflow equals inflow, perhaps only after the channel sides are overtopped and multiple outflows are thus created. The outstanding geologic example of hydraulic ponding in Washington is due to enormous Pleistocene floods from glacial Lake Missoula, which became transiently hydraulically ponded by each successive constriction in the Channeled Scabland and Columbia River Valley [J. H. Bretz *et al.*, *Geol. Soc. Am. Bull.* 67, 957 (1956); V. R. Baker, *Geol. Soc. Am. Spec. Pap.* 144 (1973); R. B. Waitt, Jr., *J. Geol.* 88, 653 (1980)].
9. The velocity of the lahar was estimated by comparison with 18 May 1980 lahars of similar magnitude, composition, and slope angle, for which velocities were computed [R. J. Janda *et al.*, in (1), p. 464].
10. One can estimate the original water content of a lahar by adding enough water to dry samples to produce a slurry that has the consistency of fluid, wet concrete. The method, although subjective, is relatively precise. A decrease in water content of only 1 to 2 percent from optimum renders the slurry too viscous to flow; an increase of 1 to 2 percent so dilutes the slurry that it cannot hold coarse particles in suspension.
11. See D. R. Crandell, *U.S. Geol. Surv. Prof. Pap.* 677 (1969).
12. R. L. Dinenart, personal communication.

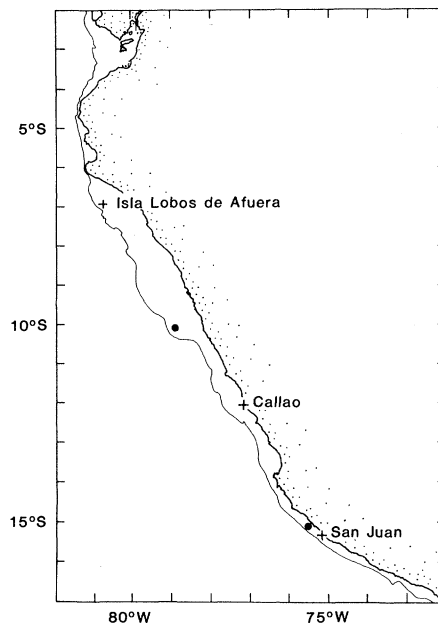
26 January 1983; revised 30 June 1983

Peru Coastal Currents During El Niño: 1976 and 1982

Abstract. *Year-long measurements of subsurface current and temperature on Peru's continental shelf included the onset of El Niño in 1976 and 1982. The Peru Coastal Undercurrent more than doubled in speed and advected anomalously warm water poleward. El Niño began in different seasons in 1976 and 1982, but the current and temperature responses were very similar. Acceleration of poleward flow at 10°S occurred several days after sea level rose at the Galápagos Islands in October 1982, suggesting the onset of El Niño propagated as a Kelvin wave.*

El Niño is, among other things, the appearance of anomalously warm water along the coasts of Ecuador and Peru, with disastrous ecological and economic consequences. Its causes and effects have been traced at least as far as the western equatorial Pacific (1-3), but its manifestations are especially dramatic in the Peruvian littoral (4). Neither the 1976 nor 1982 El Niño was predicted, but long-term measurements of subsurface current and temperature recorded the onset of El Niño on Peru's continental shelf (Fig. 1) in both years. Although the measurements were obtained at different locations and depths on the shelf (55 m below the surface over the 120-m isobath at 15°S during March 1976 to May 1977; 100 m below the surface over the 150-m isobath at 10°S during November 1981 to January 1983), both were in the Peru Undercurrent, which flows poleward (southeastward) along the coast. This poleward flow occurs over the continental shelf and slope (5), just beneath the layer of water driven equatorward and offshore by the wind, supplying the water that upwells along the coast of central

Peru (6). The time series of subsurface temperature, current, and coastal wind are shown in Figs. 2 and 3 (7). Except for warming occurring in different seasons, the time series are remarkably similar



(8). The coastal winds were persistently favorable for coastal upwelling (6), and increased during the warming phases (9).

To place these measurements in temporal and climatological perspective, the monthly mean sea surface temperatures (SST's) at Callao (12°S) are shown in Fig. 4. In a normal year, seasonal warming begins around October and continues until March. However, El Niño occurs at irregular intervals of several years (1, 2). The associated anomalous warming along the Peruvian coast usually begins in February or March after anomalous weakening of the westward trade winds in the western and central equatorial Pacific starting the previous October or November (1, 2). This sequence occurred in late 1975 and early 1976, but in 1982 the equatorial trade winds severely weakened in the early part of the year (2) and anomalously strong warming began along the coast in October 1982.

The onset of El Niño conditions in 1976 and 1982, apparent in the monthly SST data and in the subsurface temperature time series, coincided with increased poleward flow. In 1976 the temperature at 55 m rose by 3.5°C (from 13.6° to 17.1°C) during the first 64 days of the time series (27 March to 30 May); the mean alongshore current was 23.2 cm sec⁻¹ poleward during that period. In contrast, during a comparable period after the return to nearly normal conditions (the last 64 days of the time series almost 1 year later: 10 March to 13 May 1977), the temperature remained near 15°C and the mean alongshore current was only 8.8 cm sec⁻¹ poleward. In 1982 the temperature 100 m below the surface at 10°S rose 5.7°C (from 15.0° to 20.7°C) during the 64 days from 7 October to 10 December; during that period the mean alongshore current was 25.3 cm sec⁻¹ poleward. During an equivalent period nearly 1 year earlier (23 November 1981 to 26 January 1982), the temperature increased less than 1°C from 13.8°C and the alongshore current was only 4.4 cm sec⁻¹ poleward.

The anomalous warming in 1976 and 1982 was gradual and continuous for at least 4 months, and the current was strongly poleward from the beginning of the warming. This suggests that the subsurface warming was the result of advection by the poleward current. The temperature increase ($\partial T/\partial t$) of roughly

Fig. 1. Current meter locations off Peru (two bold dots) and the 200-m isobath, approximate edge of the continental shelf. Winds were measured at Isla Lobos de Afuera and San Juan and SST's were measured at Callao.

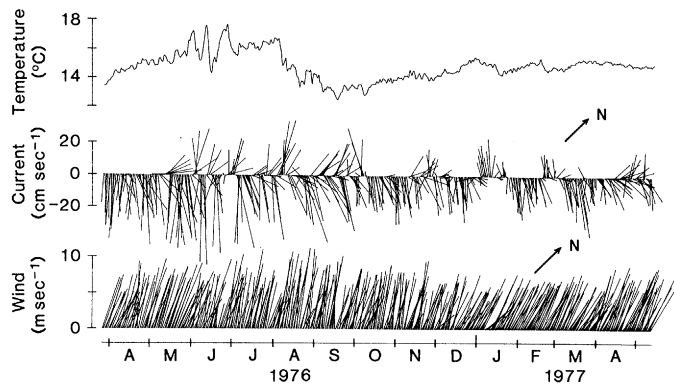


Fig. 2. Temperature and current measured 55 m below the surface at 15°S, and the coastal wind at San Juan (7). The vertical axes denote the alongshore direction. The direction of north is indicated by an arrow of length equivalent to 20 cm sec⁻¹ in current and 5 m sec⁻¹ in wind.

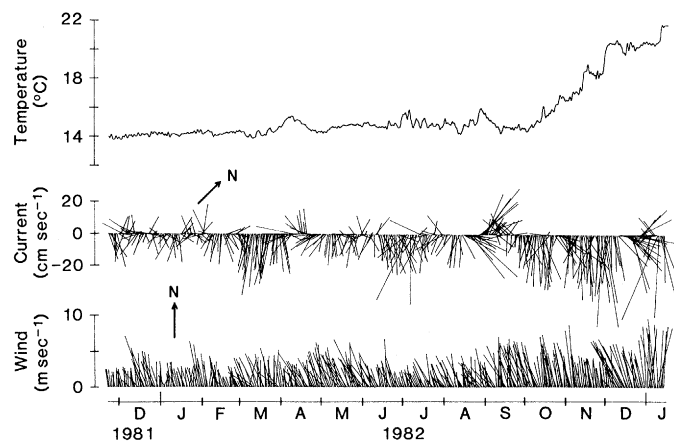


Fig. 3. Temperature and current measured 100 m below the surface at 10°S, and the wind measured on Isla Lobos de Afuera. Axes, scales, and so forth are as in Fig. 2.

0.1°C per day observed at 100 m in late 1982 would result from advection [$v(\partial T/\partial y)$] by the observed current, $v \sim 25$ km per day, if the temperature gradient ($\partial T/\partial y$) were about 4°C in 1000 km—a not unreasonable value. With the data at hand, the source of this anomalously warm water at 10°S is a matter of speculation. In mid-February 1983 the water at the location of the current meter was about 20.4°C with a salinity of about 35.1 per mil; at the same depth (100 m) farther seaward over the slope at 10°S, the temperature was nearly the same but the salinity was over 35.4 per mil; and at 85°W on the equator the temperature at 100 m was 21.0°C and the salinity was 35.04 per mil (10). Advection from the equator is thus a possibility, as was suggested by Lukas (11) in his analysis of historical hydrographic data.

The onset of El Niño at 10°S in early October 1982 was sudden. The date of 7 October marks a watershed: the temperature at 100 m, which had averaged 14.98°C over the preceding 64 days, in-

creased to above 15°C on 7 October and did not fall below that temperature during the remainder of the time series record. The alongshore current averaged over 1, 8, and 64 days before 7 October was poleward at 18.9, 18.0, and 4.2 cm sec⁻¹, respectively. Mean alongshore current abruptly accelerated to 35.8 cm sec⁻¹ poleward on 7 October, and cur-

rent averaged over the following 8 and 64 days remained poleward at 30.1 and 25.3 cm sec⁻¹. The rapid poleward acceleration is suggestive of a propagating Kelvin wave. Wyrтки (12), in discussing sea level in the equatorial Pacific in 1982, stated: "At Santa Cruz [Galápagos Islands] sea level does not start to rise until the end of August, but the really steep increase, which indicates the leading edge of the large Kelvin wave, occurs only around October 1." If the rapid rise in sea level at Santa Cruz (1°S, 90°W) about 1 October were the signature of a first-mode baroclinic Kelvin wave, the signature would travel at about 200 to 240 km per day eastward to South America and then poleward along the continental margin, passing through the mooring location at 10°S, 79°W (13). The equatorial and low-latitude shelf wave guides are wide, and the path the signal would follow between Santa Cruz and the shelf mooring at 10°S would be longer than the great circle distance (1500 km) but shorter than the path hugging the equator and coastline (2100 km). The arrival time of "the leading edge of the large Kelvin wave" at 10°S would thus be between 6 and 10 October, and would be marked by a rapid poleward acceleration in the current. This is what the time series at 10°S show. The elevated sea level and the increased poleward flow will presumably persist until causes analogous to, but in the opposite sense of those causing El Niño, occur (3). The measurements at 10°S are continuing to be made; one hopes that they will soon record the ending of El Niño.

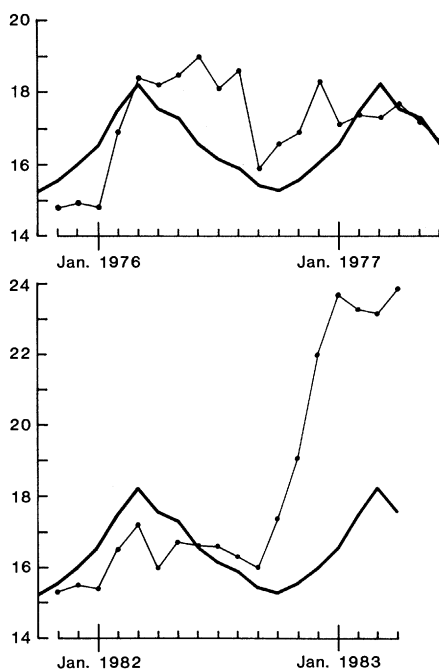
ROBERT L. SMITH

School of Oceanography, Oregon State University, Corvallis, Oregon 97331

References and Notes

1. K. Wyrтки, *J. Phys. Oceanogr.* **5**, 572 (1975); E. M. Rasmusson and T. H. Carpenter, *Mon. Weather Rev.* **10**, 354 (1982).
2. S. G. H. Philander, *Nature (London)* **302**, 295 (1983).
3. A. J. Busalacchi and J. J. O'Brien [*J. Geophys. Res.* **86**, 10,901 (1981)] have modeled the onset and persistence of El Niño.
4. C. P. Idyll, *Sci. Am.* **228**, 22 (June 1973).
5. C. Brockmann, E. Fahrbach, A. Huyer, R. L. Smith, *Deep-Sea Res.* **27**, 847 (1980).
6. B. K. Hartline, *Science* **208**, 38 (1980).
7. The original data series were low-pass-filtered (half-power point at 2 days) to reduce diurnal fluctuations to less than 1 percent amplitude. The filtered values at 1200 universal time are used in the text and figures. The alongshore orientation was determined by computing the principal axes of each vector series, the direction of maximum variance being defined as the alongshore direction.
8. The current records each had a vector mean speed of 10.8 cm sec⁻¹ directed poleward: toward 114°T at 15°S and toward 132°T at 10°S (°T indicates compass direction relative to true north).
9. Coastal upwelling continues during El Niño, but the water upwelled is much warmer, and presumably poorer in nutrients, than normal. An explanation for increased coastal winds during El Niño is given by D. B. Enfield, *J. Geophys. Res.* **86**, 2005 (1981).
10. A. Huyer, unpublished results.

Fig. 4. Monthly mean SST's measured at La Punta in Callao. The bold lines are monthly mean SST's averaged for 26 years (1956 to 1981). The monthly mean SST's starting in November prior to the El Niño years discussed in this report (1976 and 1982) are shown by dots connected by light lines.



11. R. Lukas, thesis, University of Hawaii (1981).
12. K. Wyrski, *Trop. Ocean Atmos. Newsl. No. 16* (1983), p. 6 (available from the Joint Institute for the Study of Atmosphere and Ocean, University of Washington, Seattle 98195).
13. The dynamics of Kelvin waves in this context are discussed by A. E. Gill (*Atmosphere-Ocean Dynamics* (Academic Press, New York, 1982)). Observational evidence for equatorial and coastal Kelvin waves in the eastern Pacific, with estimates of their phase speed, has been given by R. A. Knox and D. Halpern [*J. Mar. Res.* **40**, 329 (1982)] and R. D. Romea and R. L. Smith (*J. Phys. Oceanogr.*, in press), respectively.
14. This research and the continuation of measurements at 10°S are supported by NSF grant OCE-8017929. I am indebted to D. Hansen and A. Leetmaa for enabling the measurements at 10°S to be started in 1981 with National Oceanic and Atmospheric Administration research vessels; to W. Garcia-A., H. Soldi-S., and S. Zuta for the coastal wind and SST data; and to D. B. Enfield and A. Huyer for helpful discussions. The measurements at 15°S during 1976 and 1977 were a part of the coastal upwelling ecosystem analysis study supported by NSF.

26 May 1983; revised 1 August 1983

Stereospecific Action of Pyrethroid Insecticides on the γ -Aminobutyric Acid Receptor-Ionophore Complex

Abstract. *The potent α -cyano-3-phenoxybenzyl pyrethroids, including cypermethrin, deltamethrin, and fenvalerate, act stereospecifically to inhibit binding to rat brain synaptic membranes of sulfur-35-labeled t-butylbicyclophosphorothionate, a new radioligand for the picrotoxinin binding site. Scatchard analysis indicates that picrotoxinin inhibition of t-butylbicyclophosphorothionate binding is competitive whereas cypermethrin inhibition possibly involves a closely associated site in the γ -aminobutyric acid receptor-ionophore complex. Studies with 37 pyrethroids reveal an absolute correlation, that is, no false positives or negatives, between mouse intracerebral toxicity and in vitro inhibition: all toxic cyano compounds but none of their nontoxic stereoisomers are inhibitors; cis isomers are more potent than trans isomers as both toxicants and inhibitors; and noncyano pyrethroids are much less potent or are inactive.*

Pyrethroid esters of (S)- α -cyano-3-phenoxybenzyl alcohol with various 3-substituted-2,2-dimethylcyclopropanecarboxylic acids (such as cypermethrin and deltamethrin) or 2-substituted-3-methylbutyric acids (such as fenvalerate) are potent and widely used insecticides (Fig. 1) (1). The poisoning syndrome of these pyrethroids is referred to as type 2 to differentiate it from the apparently different symptomology and mode of action for the earlier pyrethroids, referred to as type 1 (2-6). Unique type 2 features for the neurotoxicity of the cyanophenoxybenzyl esters are (i) inactivity in inducing repetitive firing after stimulation of the cockroach cercal sensory nerve (3); (ii) primary action in the central nervous system of mammals (4); (iii) prominent symptoms of sinuous writhing and profuse salivation in mammals (5); and (iv) delay by diazepam of the symptoms of poisoning (6). The type 1 pyrethroid action is similar in many respects to that of DDT (3, 7) but the type 2 syndrome of intracerebrally administered pyrethroids more closely approximates that of the convulsant picrotoxinin (PTX) (4, 6). Deltamethrin and a variety of cage convulsants, including bicyclophosphorus esters, inhibit binding of [³H]dihydropicrotoxinin (the dihydro derivative of PTX shown in Fig. 1) to rat brain synaptic membranes, whereas the essentially nontoxic α R epimer of deltamethrin is inactive (8). These observations suggest a possible relation between

the type 2 pyrethroid action and the γ -aminobutyric acid (GABA) receptor complex, but a more definitive approach is needed. We find, by using a new radioligand for the PTX binding site, namely [³⁵S]t-butylbicyclophosphorothionate, or [³⁵S]TBPS, (Fig. 1) (9), that (S)- α -cyanophenoxybenzyl esters act as

inhibitors in a stereospecific manner related to their toxicity by binding to a site closely associated with but possibly distinct from that of TBPS and PTX.

The binding of [³⁵S]TBPS (10) was recently characterized by using rat brain synaptic membranes treated with EDTA and dialyzed to remove endogenous GABA (9). Similar results are obtained with our standard procedure (Fig. 2) using undialyzed membranes with respect to pH and temperature dependence, drug specificity and potency, and percent specific binding. TBPS binding is apparently to a single population of high-affinity sites (linear Scatchard plot) and is inhibited competitively by PTX, that is, the dissociation constant (K_d) increased with no change in the maximum number of binding sites (B_{max}) (Fig. 2B), supporting the earlier indications that PTX and TBPS bind to the same site (9). Like PTX, the bicyclophosphates (11) are indirect or noncompetitive GABA-A antagonists (9, 12). Inhibition by (1R, α S)-cis-cypermethrin of TBPS binding, on the other hand, appears to be mixed or possibly noncompetitive (it increases K_d and decreases B_{max} , although in neither case to a significant extent) (Fig. 2B). This suggests that the pyrethroid binding domain may be distinct from that of TBPS and PTX or that they only partially overlap. Inhibition of binding is concentration-dependent with both PTX and (1R, α S)-cis-cypermethrin, and although complete for PTX, it is maxi-

Table 1. Stereospecific correlation between in vitro potency of α -cyano-3-phenoxybenzyl pyrethroids as inhibitors of [³⁵S]TBPS binding and their toxicity. Inhibitory potencies (standard error < 10 percent of the mean; N = 6) are relative to (1R, α S)-cis-cypermethrin at 5 μ M, which gave 37 percent inhibition (assays as in legend to Fig. 2 but at 2 to 3 nM [³⁵S]TBPS and 0.5 mg of protein per milliliter). Total and nonspecific binding in the controls were typically about 3000 and 350 count/min, respectively. Toxicities are also relative to (1R, α S)-cis-cypermethrin with a mouse intracerebral LD₅₀ of 1.4 nmole per gram of brain tissue determined by injection in 3 μ l of methoxytriglycol into the third ventricle [data from (4) or determined by an identical procedure]. Values tabulated as 0 for inhibition are < 5 and for toxicity are < 0.1. Deltamethrin was not assayed as the S-acid isomers. Comparable values (relative binding, toxicity) for pyrethroids with other types of acid moieties are: (1R, α S)-cis-cyphenothrin (54, 14) (1R, α S)-trans-cyphenothrin (31, 7) and (RS)-fenpropathrin (56, 11). The isomers indicated by asterisks are potent insecticides and the other isomers are essentially inactive (1, 2).

Pyrethroid	Assay	Relative potency		
		S-alcohol		R-alcohol
		R-acid	S-acid	R- and S-acid
<i>3-(2,2-Dihalovinyl)-2,2-dimethylcyclopropanecarboxylates</i>				
cis-Cypermethrin	Inhibition	100*	0	0
	Toxicity	100*	0	0
trans-Cypermethrin	Inhibition	54*	0	0
	Toxicity	43*	0	0
Deltamethrin	Inhibition	73*		0
	Toxicity	57*		0
<i>2-Substituted-3-methylbutyrates</i>				
Fenvalerate	Inhibition	0	43*	0
	Toxicity	0	57*	0
Fluvalinate	Inhibition	50*	0	
	Toxicity	34*	0	